Sources of Functional Apparent Diffusion Coefficient Changes Investigated by Diffusion-Weighted Spin-Echo fMRI

Tao Jin,[1*] Fuqiang Zhao,[2] and Seong-Gi Kim[1,2]

The mechanism behind previously observed changes in the apparent diffusion coefficient (ADC) during brain activation is not well understood. Therefore, we investigated the signal source and spatial specificity of functional magnetic resonance imaging (fMRI) ADC changes systematically in the visual cortex of cats using diffusion-weighted (DW) spin-echo (SE) fMRI with *b*-values of 2, 200, and 800 s/mm^2, and echo times (TE) of 16, 28, and 60 ms at 9.4 T. For $b \geq 200$ s/mm^2, no ADC changes were detected in brain parenchyma, suggesting a minimal tissue contribution to the ADC change. For $b \leq 200$ s/mm^2, TE-dependent ADC increases were observed. When the venous blood contribution was minimized, the ADC change was higher at the middle cortical layer than at the cortical surface, which is mainly attributed to a functional elevation in arterial blood volume. At TE = 16 ms, the highest ADC changes occurred at the cortical surface with its large draining veins, which can mainly be explained by an additional contribution from the venous blood oxygenation changes. Our TE-dependent ADC results agree with computer simulations based on a three-compartment model. The contribution of arterial blood volume changes in ADC fMRI offers an improvement in spatial localization for SE-BOLD fMRI studies. Magn Reson Med 56:1283–1292, 2006.

Key words: ADC; diffusion weighting; BOLD; spin echo; IVIM; high field

The blood oxygenation level-dependent (BOLD) technique is widely used in functional MRI (fMRI) research because of its high sensitivity and easy implementation (1–3). Since the BOLD signal source includes various deoxyhemoglobin-containing vascular networks ranging from small capillaries to large draining veins, the spatial localization of BOLD signal can be distant from the actual sites of neural activity. To overcome this shortfall of BOLD fMRI, measurement of the apparent diffusion coefficient (ADC) of brain water has been suggested as an alternative approach to detect stimulation-induced signal changes (4–9).

The measurement of ADC in fMRI is generally achieved by varying the levels of diffusion weighting (usually quantified as *b*) and then fitting the resulting attenuated signals to a monoexponential decaying function of *b*. According to the intravoxel incoherent motion (IVIM) weighting model (10), when the *b*-values are small (e.g., $b < 200$–300 s/mm^2), the ADC contrast mainly comes from the vascular network because the fast-moving proton spins in blood are attenuated to much larger extent by the diffusion/IVIM weighting gradients than the tissue water spins. Increasing the magnitude of diffusion weighting progressively attenuates the intravascular signals from larger to smaller vessels, and therefore ADC contrast can be sensitive to different compartments of water motion depending on the choice of *b*-values. Since high *b*-values (e.g., $b >$ 200 s/mm^2) mostly eliminate the intravascular signal, any detectable ADC change will likely occur in the extravascular (EV) space. A small transient decrease of ~0.8% in ADC was observed at 1.5 T by Darquie et al. (9) in this regime with slightly different temporal characteristics compared to the BOLD response. The mechanism of this ADC contrast was hypothetically attributed to neuronal cell swelling during activation. In a recent report (11), this transient ADC decrease was found to be caused by a small dilation (~1.7%) of the slow water diffusion pool and correspondingly a volume decrease in the fast water diffusion pool at the EV space, and was much faster (~2.4 s) than the BOLD response. If this ADC decrease could be confirmed to originate from a cellular level, it could potentially offer better spatial localization of brain activation than hemodynamic response-based BOLD contrast.

Song and colleagues (4–6,12–14) extensively studied ADC changes using small diffusion weightings, and found an 8–15% increase of ADC during visual stimulation in human brain at 3 and 4 T. Since the ADC response is slightly faster (~1 s) than that of BOLD, the source of these ADC increases was mainly attributed to an increase of blood flow in the arterioles and capillaries (4). However, the ADC measured in a voxel by a diffusion-weighted (DW) spin-echo (SE) or gradient-echo (GE) sequence is related to the ADC values of tissue and arterial and venous blood water, as well as their respective volume fractions and relaxation times (T_2 or T_2*). Therefore, changes in these parameters for any of the three compartments could lead to a functional ADC change. Thus, it is crucial to examine the nature of functional ADC changes and the spatial specificity of ADC-based fMRI.

In the present study we measured the ADC response using a DW SE echo-planar imaging (EPI) technique at echo times (TEs) of 16, 28, and 60 ms, and diffusion weightings of 2, 200, and 800 s/mm^2 in a well-established cat visual stimulation model at 9.4 T. One distinct advantage of using SE at 9.4 T is that one can substantially vary the contribution of the venous BOLD signal change by

[1]Magnetic Resonance Research Center, Department of Radiology, University of Pittsburgh, Pittsburgh, Pennsylvania, USA.
[2]Department of Neurobiology, University of Pittsburgh, Pittsburgh, Pennsylvania, USA.
Grant sponsor: National Institutes of Health; Grant numbers: EB003324; EB003375; NS44589; RR17239.
*Correspondence to: Tao Jin, Magnetic Resonance Research Center, Department of Radiology, University of Pittsburgh, 3025 E. Carson St., Pittsburgh, PA 15203. E-mail: taj6@pitt.edu
Received 2 June 2006; revised 21 July 2006; accepted 3 August 2006.
DOI 10.1002/mrm.21074
Published online 18 October 2006 in Wiley InterScience (www.interscience.wiley.com).

changing the TE (15), which is not easily done at lower fields. Because of the short T_2 value (~6 ms) of venous blood, the venous signal change is negligible at relatively long TE values (>40 ms), while it can be easily detectable at short TE values (<20 ms). Therefore, the application of different diffusion weightings (*b*-values) could separate the ADC changes from the blood and tissue pools, and the application of different TEs could separate the ADC changes from the arterial and venous blood pools. Additionally, a high in-plane spatial resolution of ~0.3 mm in our animal studies allowed separation of the middle cortical region from the surface of the cortex, which has large draining veins. This also helped us to determine the signal source and spatial specificity of fMRI ADC changes. The results of the ADC changes were compared with BOLD results and computer simulations based on a three-compartment model.

MATERIALS AND METHODS

Three-Compartment Model of the ADC Change

It is assumed that the MR signal in an imaging voxel consists of signals from tissue and arterial and venous blood pools. In SE studies of diffusion, the MR signal is a sum of these three pools weighted by their volume fraction, T_2 value, and DW attenuation. According to the IVIM model, the DW attenuation of the blood signal depends on the vascular structures and the flowing characteristics in blood vessels (16). For simplicity, the signal attenuations of both arterial and venous blood are assumed to be mono-exponential, with D_a^* and D_v^* ($D_a^* > D_v^*$) representing the pseudo-diffusion coefficients of arterial and venous blood, respectively. In an SE image with diffusion weighting (*b*), the signal intensity at a TE, $S(TE, b)$, can be described as

$$S(TE,b) = \exp(-b\cdot ADC) = \lambda\cdot(1 - V_a - V_v)\cdot\exp(-b\cdot D)\cdot\exp(-TE\cdot R_{2,t}) + V_a\cdot\exp(-b\cdot D_a^*)\cdot\exp(-TE\cdot R_{2,a}) + V_v\cdot\exp(-b\cdot D_v^*)\cdot\exp(-TE\cdot R_{2,v}), \quad [1]$$

where V_a and V_v are the fractional arterial and venous blood volumes (expressed in percentage), respectively; λ is the ratio between water contents of tissue and blood; D is the diffusion coefficient of tissue water; and $R_{2,t}$, $R_{2,a}$, and $R_{2,v}$ are the R_2 ($=1/T_2$) value of tissue and arterial and venous blood, respectively. The capillary blood volume is divided into arterial and venous blood pools, and any T_1 differences between tissue and blood water are ignored in this model.

The ADC value can be determined from data with two different diffusion weightings b_1 and b_2 ($b_1 < b_2$) as

$$ADC = \frac{1}{b_1 - b_2}\ln\frac{S(b_2)}{S(b_1)}. \quad [2]$$

From Eq. [1], the measured ADC is a weighted function of D, D_a^* and D_v^*, and the weighting of each individual pool is also dependent on the T_2, TE, and *b*-values. Especially in the small *b*-value regime (e.g., $b \le 200$ s/mm^2), the relative contributions of D_a^* and D_v^* to ADC are quite significant. In fMRI, stimulation-induced changes in ADC can be expressed as

$$\Delta ADC = \frac{1}{b_1 - b_2}\ln\left(\frac{1 + \Delta S(b_2)/S(b_2)}{1 + \Delta S(b_1)/S(b_1)}\right) \approx \frac{1}{b_2 - b_1}\left[\frac{\Delta S(b_1)}{S(b_1)} - \frac{\Delta S(b_2)}{S(b_2)}\right], \quad [3]$$

where $\Delta S(b_1)/S(b_1)$ and $\Delta S(b_2)/S(b_2)$ are stimulation-induced BOLD fractional signal changes with diffusion weightings of b_1 and b_2, respectively. In Eq. [3] the logarithmic relationship is expanded into a combination of linear relationships because the fractional signal changes are usually very small. Equation [3] shows that during brain activation, the *absolute* change of ADC is directly related to the difference in fractional signal changes of DW BOLD signals, $\Delta S(b)/S(b)$.

An ADC change during activation is obviously related to any changes in the diffusion coefficients D, D_a^* and D_v^*. In addition to changes in water mobility, changes in the fractional blood volume (V_a, V_v) and relaxation rate ($R_{2,v}$) also modulate the relative weightings of arterial and venous pools, and consequently the measured ADC. To obtain insight into the signal source of the functional ADC change, we performed computer simulations based on Eqs. [1] and [3]. Blood T_2 was calculated from a formula based on the Luz-Meiboom exchange model (15,17):

$$R_{2,v} = \frac{1}{T_{2,v}} = 24 + 1125(1 - Y)^2 \times\left(1 - \frac{2\tau_{ex}}{TE}\tanh\frac{TE}{2\tau_{ex}}\right)\Big/\left(1 - \frac{2\tau_{ex}}{40}\tanh\frac{40}{2\tau_{ex}}\right), \quad [4]$$

where Y is the oxygenation level of blood. In our anesthetized animal study with ~33% O_2 inhalation, Y is assumed to be 0.65 during baseline, which is slightly higher than the value of 0.55–0.6 observed during normal awake conditions (18). τ_{ex} is the correlation time of water exchange between erythrocyte and plasma, which ranges from 1 to 10 ms (19–21), and was assumed to be 1 ms here. Two *b*-values of 2 and 200 s/mm^2 used in experimental studies were employed for three different types of simulations: 1) To estimate the individual effect of one physiological parameter change on the ADC response, one of the parameters ΔV_a, ΔV_v, or ΔY was varied with all other parameters fixed at the values listed in Table 1. 2) To observe the effect of baseline V_v on the ADC change, variation of baseline V_v was simulated with a fixed blood oxygenation level change (ΔY) of 0.05. 3) The increase in blood velocity during brain activation may either increase or decrease the ADC depending on vascular characteristics (5). Here the ADC response was simulated with variations in baseline D_a^* and D_v^* values and a fixed functional increase of 50% in D_a^* and D_v^*.

Animal Preparation and Stimulation

A total of 13 female adolescent cats were studied under an animal protocol approved by the Institutional Animal Care and Use Committee at the University of Pittsburgh. Details

Table 1
Parameter values in three-compartment model simulations

Parameter	Description	Value/units
Baseline parameters		
τ_{ex}	Average exchange time	1 ms[a]
λ	Water content ratio between tissue and blood	1.03[b]
D	Diffusion coefficient of tissue water	0.8×10^{-3} mm^2/s
D_a^*	Pseudo-diffusion coefficient of arterial blood	20–150 (default 100) $\times 10^{-3}$ mm^2/s[c]
D_v^*	Pseudo-diffusion coefficient of venous blood	10–40 (default 20) $\times 10^{-3}$ mm^2/s[c]
V_a	Baseline fractional arterial blood volume	1.3%
V_v	Baseline fractional venous blood volume	2–5% (default 3.5%)
Y	Baseline blood oxygenation level	0.65[c]
R_2	Baseline tissue relaxation rate	25 s^{-1}[d]
Stimulation-induced changes		
ΔV_a	Fractional arterial blood volume change	0.1–0.4%
ΔV_v	Fractional venous blood volume change	0.1–0.4%
ΔY	Functional blood oxygenation change	0.025–0.1
$\Delta D_a^*/D_a^*$	Percentage change in D_a^*	50%
$\Delta D_v^*/D_v^*$	Percentage change in D_v^*	50%

[a]From references 38 and 19.
[b]From reference 39.
[c]See text in the "Three-Compartment Model of the ADC Change" section.
[d]From reference 40.

of the animal preparation procedure were described previously (15). Briefly, the animals were intubated and artificially ventilated under 0.8−1.2% isoflurane in a 2:1 air:O_2 mixture. The cephalic vein was cannulated to deliver pancuronium bromide (~0.2 mg/kg/h). The end-tidal CO_2 level was kept within 3.5% ± 0.5% by adjusting the respiration rate and volume, and the rectal temperature was controlled at 38.5°C ± 0.5°C using a water circulating pad. The animal's head was fixed with an in-house-made head frame with bite and ear bars. Each animal was scanned for 4−6 hr inside the magnet.

The animals were presented binocularly with high contrast drifting square-wave gratings during the stimulation condition. The temporal and spatial frequencies of the gratings were two cycles/s and 0.15 cycle/degree. Stationary gratings of the same spatial frequency were presented during the control condition. This stimulation paradigm has been routinely used to detect neural activities related to moving gratings (22).

MR Experiments

All MR experiments were carried out on a 9.4 T/31-cm horizontal magnet (Magnex, UK) interfaced to a Unity INOVA console (Varian, Palo Alto, CA, USA). The actively shielded 12-cm-diameter gradient insert (Magnex, UK) operates at a maximum gradient strength of 40 gauss/cm and a rise time of 130 μs. A 1.6-cm-diameter surface coil was placed on top of the animal's head for radiofrequency (RF) excitation and reception. Fast low-angle shot (FLASH) images were obtained to identify anatomical structures in the brain and to place the region of interest (ROI) close to the isocenter of the magnetic field. Magnetic field homogeneity was optimized by localized shimming over a ~$10 \times 5 \times 5$ mm^3 volume to yield a water spectral linewidth below 25 Hz. From multislice "scout" GE-EPI BOLD fMRI studies, a single 2-mm coronal slice perpendicular to the surface of the cortex that yielded a high-quality EPI image and robust BOLD contrast was chosen. All subsequent experiments were conducted on that slice with a 2×2 cm^2 field of view (FOV) and 2-mm thickness. For anatomical reference, a T_1-weighted image was acquired by four-shot SE-EPI with a 128×128 matrix.

All fMRI data were acquired with a 64×64 matrix, using a double-SE EPI sequence with adiabatic half- and full-passage pulses (23). Two unipolar diffusion-weighting gradients along all three axes were placed on both sides of the second 180° pulse, and the order of the *b*-values was pseudo-randomized. To evaluate the contribution of the intravascular BOLD signal to the functional ADC change, data were acquired at three different values of TE (16, 28, and 60 ms).

For the short-TE value of 16 ms ($N = 7$ animals), the accommodation of diffusion-weighting gradients in a single-shot EPI sequence is not feasible; therefore, a two-shot SE-EPI with center-out *k*-space sampling was used. The repetition time (TR) = 2 s (1 s for each shot), the gradient pulse duration (δ) = 2 ms, and the time interval between the two gradient pulses (Δ) = 7 ms. In each run, two *b*-values of 2 and 200 s/mm^2 were arrayed, for a temporal resolution of 4 s. The 800 s/mm^2 was not sampled for TE = 16 ms. For experiments with TE = 28 and 60 ms ($N = 6$ animals), single-shot EPI was used with shifted echo acquisition to reduce the effective TE (Fig. 1C in Ref. 24), where the zero *k*-space line was shifted by 24 lines from the center (echo center located at the eighth line of the *k*-space). Other parameters were TR = 1.2 s, $\delta = 3$ ms, and $\Delta = 13$ ms. Although the different EPI acquisition schemes for short TE (16 ms) and long TE (28 and 60 ms) may have different image distortion characteristics, the effect on our results will be small since we performed an ROI-based analysis of functional signal percentage changes, and the short- and long-TE studies were performed on separate animals. In each run, data were acquired sequentially with a series of three *b*-values of 2, 200, and 800 s/mm^2, for a

temporal resolution of 3.6 s. In each study, runs with TEs of 28 and 60 ms were interleaved. For all TE values the stimulation paradigm included 10 control, 10 stimulation, and 10 control images for each *b*-value. The stimulation duration was therefore 36 s or 40 s, and there was a 1-min rest between repetitive runs. About 20 runs were averaged to improve the signal-to-noise ratio (SNR). Because of time restrictions, studies with TE = 16 ms were performed separately from those from TE = 28 and 60 ms.

fMRI Data Analysis

Data were analyzed with the use of Matlab® programs and STIMULATE software (25). Since sequential data sampling was performed, images with different *b*-values were obtained at different time points. To avoid erroneous results when analyzing the dynamic ADC signal change, images with same diffusion weighting were grouped together, and then linear temporal interpolation was performed to take into account their different time origins. For each experiment, two series of ADC images were calculated using Eq. [2]: one from images with $b = 2$ and 200 s/mm^2, and the other from images with $b = 200$ and 800 s/mm^2, which will be referred to as small and large *b*-value pairs, respectively.

Student's *t*-test was performed on a pixel-by-pixel basis to detect the activated area. A *t*-value threshold of 2 ($P < 0.03$) and a minimal cluster size of three pixels were applied. Signal percentage changes were then calculated for the statistically active pixels. For quantitative analyses, two ROIs (120–150 pixels each) were drawn based on the activation map with $b = 2$ s/mm^2 and the anatomic image: a middle cortical ROI and a cortical surface ROI were hand-traced each with 1–2 pixels thickness to encompass approximately the middle 1/3 and the surface 1/3 of the cortex, respectively. When the BOLD and ADC maps were compared, functional data with $b = 2$ s/mm^2 were used as BOLD images. TE-dependent BOLD and ADC signal percentage changes were computed within the ROIs. To calculate the signal percentage change, the baseline periods were defined as eight images (32 or 28.8 s) of prestimulation data (excluding the first and 10th images), while the activation periods were defined as data from the third to 10th images (e.g., 8–40 s or 7.2–36 s) after the onset of stimulation.

The spatial characteristics of the BOLD and ADC responses were analyzed as a function of cortical depth (26). Rectangular sections within area 18 of the visual cortex were selected first (27). Pixels were then spatially interpolated along the direction normal to the cortical surface using the nearest-neighbor resampling method (28), and finally the averaged signal profiles across cortical layers were plotted as a function of distance from the surface of the cortex. The full width at half maximum (FWHM), peak position, and peak amplitude were determined from the averaged profile. All data are reported as the mean ± standard deviation (SD) unless noted otherwise.

RESULTS

Simulations at 9.4 T With the Three-Compartment Model

Although many physiological parameters change simultaneously during stimulation, to gain a better understanding of the signal source of ADC change, we evaluated the contribution of each parameter change separately under the assumption that there were no other stimulation-induced parameter changes (see Table 1). Figure 1a and b show the ADC changes induced by ΔV_a and ΔV_v, respectively, as a function of TE. An increase in fractional arterial blood volume (ΔV_a) induces a linear increase in ADC, which is almost independent of TE (Fig. 1a). In contrast, the contribution of ΔV_v to the ADC percentage change (Fig. 1b) is negligible for TE $>$ 20 ms due to the short T_2 value of venous blood, but increases significantly at very short TE values. The contributions from a venous oxygenation level change (ΔY) are shown in Fig. 1c and d. In Fig. 1c ΔY is varied with a fixed baseline V_v value of 3.5%, whereas in Fig. 1d V_v is varied with a fixed ΔY value of 0.05. The ADC change is nearly proportional to ΔY and V_v, but is dependent on TE in both cases.

The effect of increasing arterial and venous blood velocity (or D^*) to the ADC change is related to the baseline D^* (Fig. 1e and f). The ADC change is nearly TE-independent above TE = 10 ms for arterial blood (D_a^*), whereas the effect of D_v^* is strongly TE-dependent below TE = 20 ms. A 50% increase in D_a^* reduces the functional ADC, while an increase in D_v^* can either increase or decrease the ADC for TE $<$ 20 ms (Fig. 1f). The ADC increases for baseline $D_v^* < 20 \times 10^{-3}$ mm^2/s, and decreases for other baseline D_v^* values.

Source of Stimulation-Induced ADC Changes

Figure 2 shows DW SE-BOLD percentage change maps at three TEs. For data with TE = 16 ms, the highest signal change (yellow pixels) is located at the surface of the cortex when *b* is 2 s/mm^2 (Fig. 2a), and is mostly suppressed when a diffusion weighting of $b = 200$ s/mm^2 is applied (Fig. 2b), suggesting that the major contribution to the SE-BOLD signal change is from venous blood (15). In data with TE = 28 and 60 ms (Fig. 2d–i), large regions of activation can be seen within the gray matter area (depicted by the green contour), regardless of *b*-value. This indicates that BOLD signal changes come mostly from the EV compartment. For TE = 60 ms, a slight difference between different *b*-value data was observed due to different SNRs. For TE = 28 ms, the difference in the signal change between $b = 2$ and 200 s/mm^2 is more noticeable than for TE = 60 ms because there is small intravascular BOLD signal change at this intermediate TE value (15).

Quantitative analyses were performed for the averaged percentage signal changes ($\Delta S/S$) of the surface and middle cortical ROIs (depicted by the pink and yellow pixels, respectively, in Fig. 2c), and the results are shown as a function of TE in Fig. 3a and b. At the middle cortical ROI (Fig. 3a), $\Delta S/S$ decreases as *b* increases from 2 to 200 s/mm^2 for all three TE values, while the $\Delta S/S$ at $b = 800$ s/mm^2 is almost identical to that of $b = 200$ s/mm^2 for both TE = 28 and 60 ms. At the cortical surface ROI (Fig. 3b), the difference in $\Delta S/S$ between $b = 2$ and 200 s/mm^2 is not significant for TE = 60 ms, while there is a significant difference for TE = 16 ms and TE = 28 ms. Interestingly, the $\Delta S/S$ at $b = 800$ s/mm^2 was slightly higher than that of $b = 200$ s/mm^2.

Absolute ADC changes were calculated from both ROIs at each of the three TE values using Eq. [3] (Fig. 3c). The

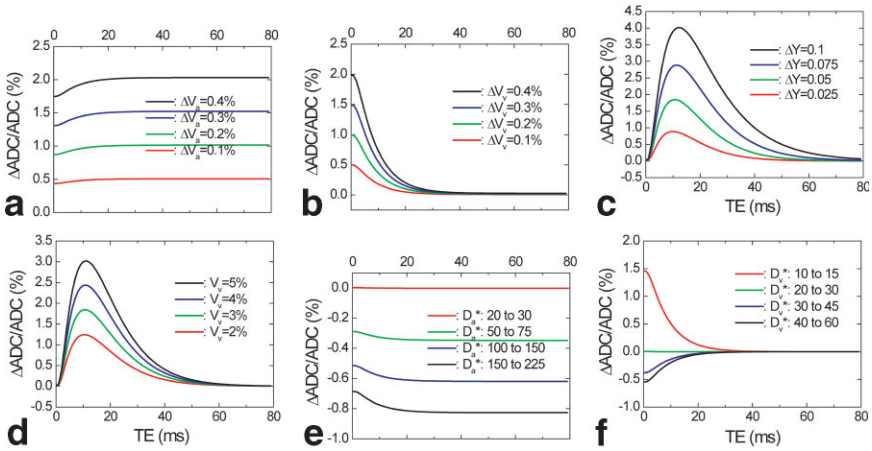

FIG. 1. Simulated percentage change of ADC as a function of TE at 9.4 T based on the three-compartment model. The ADC values were calculated from $b = 2$ and 200 s/mm^2. Parameter values for fractional arterial blood volume change ΔV_a (**a**), fractional venous blood volume change ΔV_v (**b**), blood oxygenation level change ΔY (**c**), baseline fractional venous blood volume V_v (**d**), arterial pseudo-diffusion coefficient D_a^* (units of 10^{-3} mm^2/s) (**e**), and venous pseudo-diffusion coefficient D_v^* (unit of 10^{-3} mm^2/s) (**f**) were varied, while other parameter values were fixed as listed in Table 1. In e and f, it was assumed that D_a^* and D_v^*, respectively, increase by 50% during stimulation.

stimulation-induced ADC change is not significantly different from zero at the middle cortical ROI when obtained from the large *b*-value pair for TE = 28 or 60 ms ($P > 0.09$, $N = 6$), suggesting that the contribution of tissue signals to functional ADC change is minimal. At the cortical surface, there is a very small (<0.3%) but statistically significant functional ADC decrease from the large *b*-value pair for both TE = 28 and 60 ms ($P < 0.02$). For both ROIs, ΔADC at TE = 16 ms obtained from the small *b*-value pair is significantly larger than the corresponding values at TE = 28 and 60 ms. For TE = 28 and 60 ms, ΔADC values from the middle ROI obtained from the small *b*-value pair are not statistically different ($P = 0.23$, $N = 6$). At the cortical surface, however, ΔADC is slightly larger ($P = 0.03$, $N = 6$) at TE = 28 ms than at TE = 60 ms.

In order to visualize the ADC activation, functional ADC *t*-maps were obtained from the DW data of the study shown in Fig. 2. The ADC *t*-maps calculated from the small *b*-value pair for all three TEs (Fig. 4a–c) show a functional ADC increase within the cortex, which is consistent with results from the middle cortical ROI for all animals (Fig. 3c). For the TE = 60 ms image, a Gaussian filter with an FWHM of 1.5 pixel was applied. Although a large number of activated pixels were observed in all three ADC *t*-maps, their spatial characteristics show a strong dependence on TE. For TE = 16 ms, the ADC activation is highest at the surface of the cortex, while the activated pixels with highest ADC changes appear within parenchyma for TE = 28 and 60 ms. In Fig. 4d, the ADC activation map calculated from the large *b*-value pair at TE = 28 ms has few ADC-increased pixels within the parenchyma, consistent with Fig. 3c, and also ADC-decreased pixels at the surface of the cortex. Similar results were found for TE = 60 ms (not shown).

Further insights into the functional ADC change can be obtained from its temporal characteristics. ADC dynamics will follow a typical hemodynamic response pattern if the hemodynamic response is the major source of functional ADC changes. Figure 5 shows the averaged time courses ($N = 6$) of ADC responses with TE = 28 ms in the middle cortical ROI. The baseline ADC values calculated from the small and large *b*-value pairs for the ROI are 0.92 and 0.82×10^{-3} mm^2/s, respectively. In the middle cortical ROI, the ADC response is expected to be slightly faster than the BOLD response because the BOLD signal originates mostly from small vessels on the venous side, while the ADC signal has a significant arterial blood contribution. However, our temporal resolution (3.6 s) was too

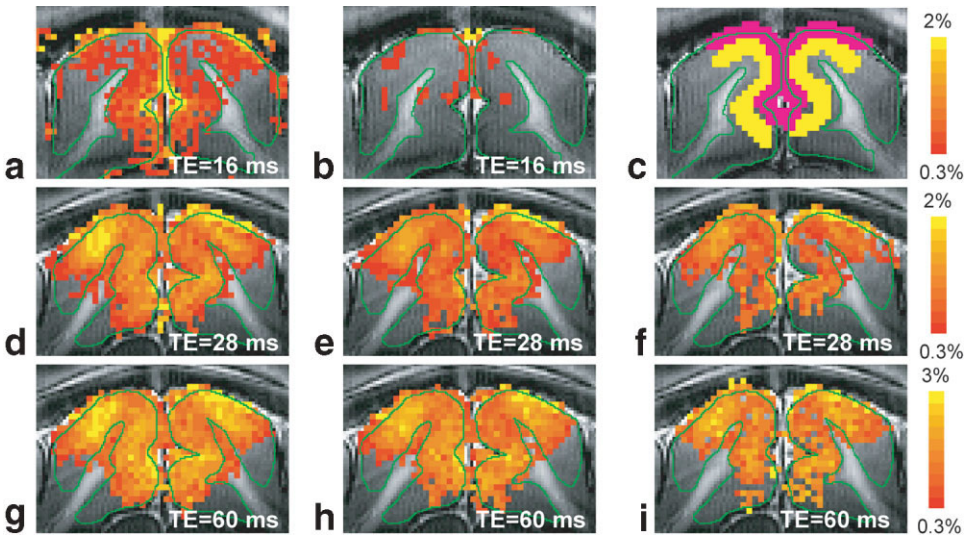

FIG. 2. DW SE-BOLD signal percentage change maps overlaid on T_1-weighted images. Results are shown for TE = 16 ms with (**a**) $b = 2$ s/mm^2 and (**b**) 200 s/mm^2 on one animal. The remaining images are from a second animal for TE = 28 ms with (**d**) $b = 2$ s/mm^2, (**e**) 200 s/mm^2, and (**f**) 800 s/mm^2, and for TE = 60 ms with (**g**) $b = 2$ s/mm^2, (**h**) 200 s/mm^2, and (**i**) 800 s/mm^2. In **c**, ROIs are shown as defined, where pink represents the cortical surface ROI and yellow represents the middle cortical ROI. All maps were calculated on pixels with *t*-value ≥ 2 and cluster size ≥ 3. Note the difference in the color bar scales for different TE values.

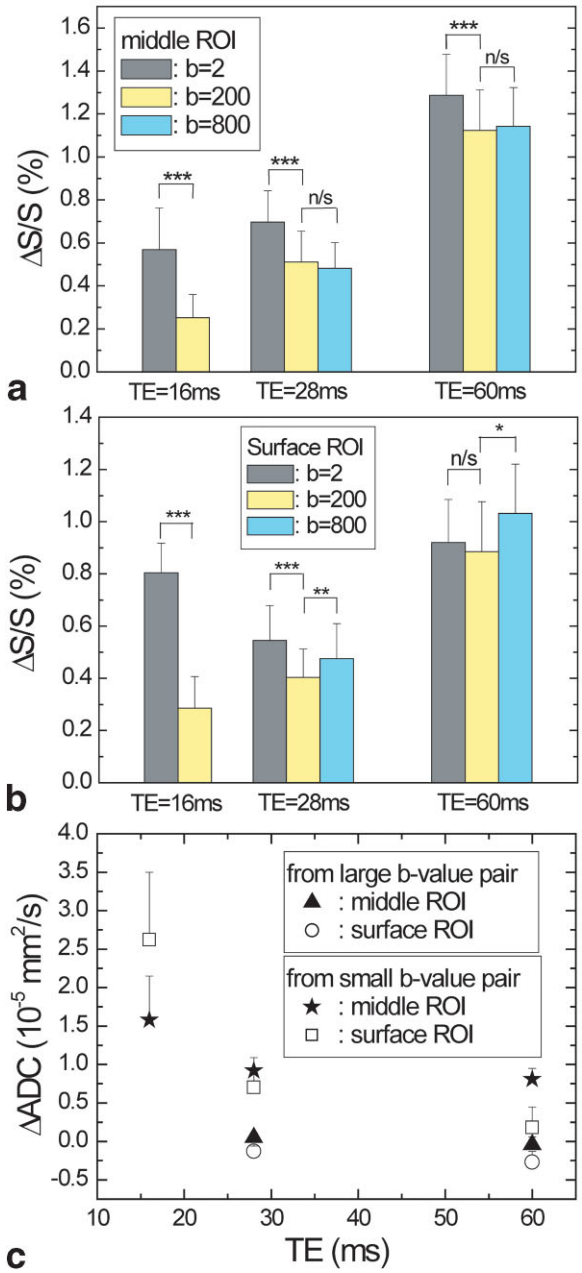

FIG. 3. Quantitative results of regional analysis ($N = 7$ for TE = 16 ms; $N = 6$ for TE = 28 and 60 ms). The BOLD signal percentage change is graphed as a function of TE for three b-values from within (**a**) the middle cortical ROI and (**b**) the cortical surface ROI. **c:** Absolute ADC change was calculated from the small and large b-value pairs for both ROIs. The paired t-test results are represented by symbols: n/s = not significant ($P > 0.05$), * $P < 0.05$, ** $P < 0.01$, and *** $P < 0.001$.

slow to detect such a difference (4). The time course of ADC calculated from the small b-value pair was very similar to the BOLD response ($b = 2$ s/mm^2), while no change was detected for the ADC data calculated from the large b-value pair.

Spatial Localization of ADC Changes

Signal profiles across the cortex were obtained to determine the spatial specificity of the ADC response. Baseline ADC values, the ΔADC/ADC calculated from the small b-value pair, and the $\Delta S/S$ values of BOLD signals ($b = 2$ s/mm^2 results) are shown as a function of cortical depth in Fig. 6, where the horizontal axis represents the distance from the surface of the cortex. The cortical thickness of the gray matter in the visual cortex is around 1.6 mm, and the upper, middle, and lower cortical regions were determined based on literature values (29). The baseline ADC values are similar for all three TE values (Fig. 6a), with values at the middle and lower cortical regions within the range of $0.85 - 0.95 \times 10^{-3}$ mm^2/s, and gradually increasing to $\sim 2 \times 10^{-3}$ mm^2/s at the surface of the cortex. This increase in the upper cortex is likely caused by the partial-volume effect of cerebrospinal fluid (CSF), which has a larger diffusion coefficient than tissue water ($\sim 2.5 \times 10^{-3}$ mm^2/s), and/or faster blood movement in the large surface vessels. For TE = 16 ms, a broad peak of ΔADC/ADC is observed at the middle of the cortex even though the highest value of ΔADC/ADC is located at the cortical surface. In contrast, the BOLD signal change for TE = 16 ms monotonically decreases with cortical depth. These large ADC and BOLD changes at the surface of the cortex are due to significant venous blood contributions. For both TE = 28 and 60 ms, ΔADC/ADC (Fig. 6b) peaks at the boundary of the middle and deeper cortical layers ($\sim$1.1 mm), slightly shifted compared to the SE-BOLD responses (Fig. 6c). The ratio of ΔADC/ADC at the middle of the cortex to that at the surface of the cortex is significantly higher than the same comparison for the BOLD signal changes (ΔS/S at the middle of the cortex is about $\sim$50% higher than at the cortical surface for TE = 28 and 60 ms data, while ΔADC/ADC at the middle of the cortex is $\sim$2 and 4 times the surface values for TE = 28 and 60 ms, respectively). The FWHM of the peak, peak position, and peak intensity of ADC, SE-BOLD, and CBV-weighted results are listed in Table 2. The FWHM of the ADC response is slightly broader than that of the CBV response, but is much narrower than that of the BOLD response ($\sim$33% for TE = 60 ms). This indicates that the spatial origin of the ADC change is better localized to the middle cortical region as compared to SE BOLD.

DISCUSSION

Since an imaging voxel in the parenchyma contains tissue and arterial and venous blood water, the measured ADC value is a weighted function of ADC values from these pools. When the signal from the venous pool is suppressed by using a long TE value at 9.4 T, only tissue and arterial blood pools contribute to the ADC. Additionally, b-values of 200 and 800 s/mm^2 will suppress the arterial blood contribution, leaving mostly signals from the tissue pool. Therefore, based on multiple TE and b-value studies, the relative contribution of these three pools to functional ADC changes can be evaluated. Our results show that 1) an ADC change in the tissue pool was not detected with our experimental settings; 2) in the small b-value regime, an arterial blood volume increase is likely to be the major source of ADC change when the venous signal contribution is removed; 3) at short TE values, the contribution of the venous signal change can be significant, even dominant at 9.4 T, and is mostly due to the venous blood

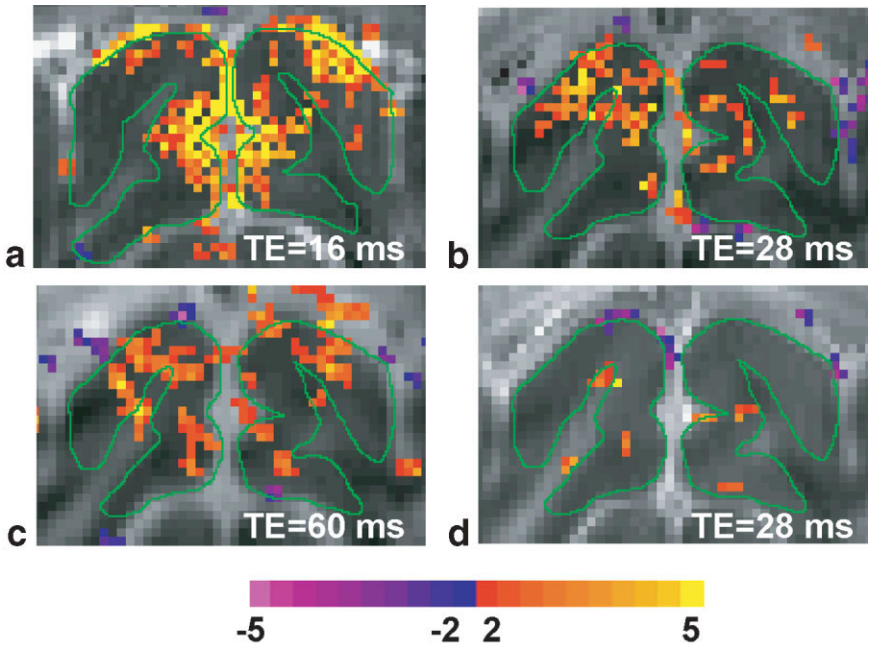

FIG. 4. Functional ADC *t*-maps. Values are calculated from the small *b*-value pair for TE = 16 ms (**a**), 28 ms (**b**), and 60 ms (**c**), and from the large *b*-value pair for TE = 28 ms (**d**). All pixels were calculated using $t \geq 2$ and cluster size ≥ 3. For the TE = 60 ms image, a Gaussian filter with an FWHM of 1.5 pixels was applied.

oxygenation level change; and 4) the ADC activation maps show better spatial localization to the middle cortical layer than the BOLD SE maps.

Origins of Functional ADC Change

Tissue

In previous studies (9,11) a small transient decrease in ADC was observed in the tissue pool and attributed to cell swelling during stimulation. In our experiments, no ADC change was detected in the tissue compartment, while very small ADC decreases (<0.3%) were observed at the cortical surface using the large *b*-value pair. Our inability to observe the ADC decrease at the parenchyma may be

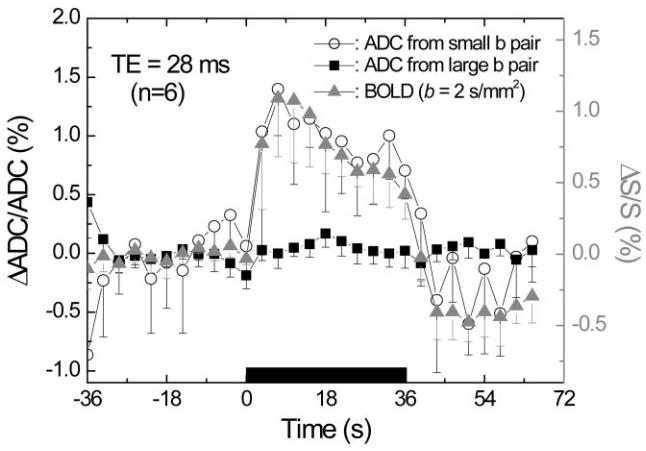

FIG. 5. Averaged time course of ADC and BOLD percentage change for TE = 28 ms at the middle of the cortex ($N = 6$). The open circles indicate ADC calculated from the small *b*-value pair, the squares indicate ADC calculated from the large *b*-value pair, and the gray triangles indicate the BOLD ($b = 2$ s/mm^2) signal percentage changes. The black bar shows the stimulation period.

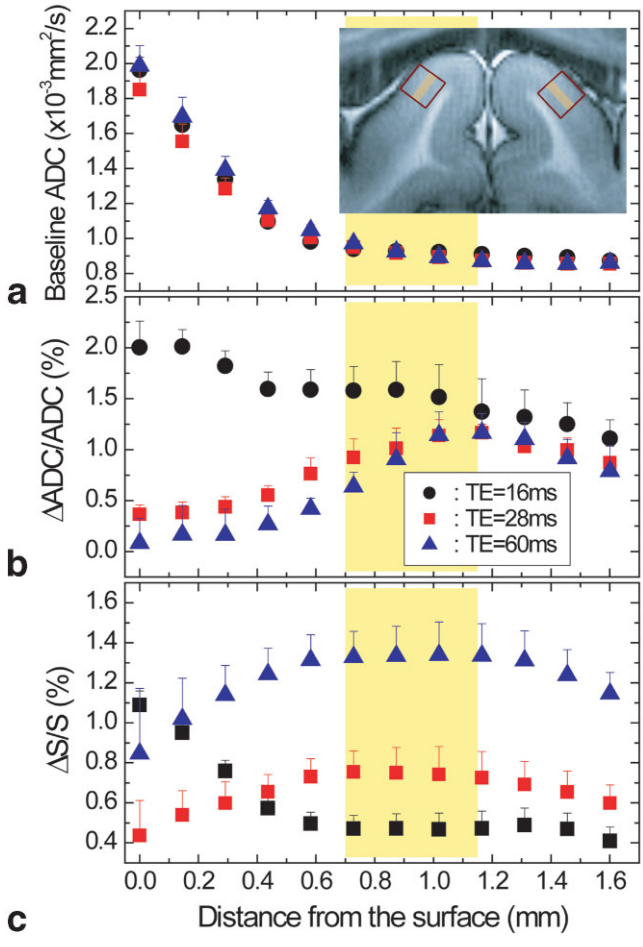

FIG. 6. Cortical depth profiles of the baseline ADC (**a**), and the ADC and BOLD percentage change (**b** and **c**) at three TEs. The choice of areas for profile calculation appears as red boxes on a T_1-weighted image in the inset in a. ADC data were calculated from $b = 2$ and 200 s/mm^2, and BOLD data were obtained from $b = 2$ s/mm^2. The yellow background represents the middle cortical layer. Data points are shown as the mean ± standard error of the mean (SEM).

Table 2
Comparison of Cortical Depth-Dependent Functional ADC, BOLD, and CBV Changes

	FWHM (mm)	Peak position (mm)	Peak intensity (%)
ΔADC/ADC (TE = 28 ms)	1.05	1.10	1.17
ΔADC/ADC (TE = 60 ms)	0.96	1.12	1.17
ΔS/S (SE-BOLD, TE = 28 ms)	1.33	0.97	0.74
ΔS/S (SE-BOLD, TE = 60 ms)	1.42	0.99	1.34
ΔCBV/CBV (GE)[a]	0.92 ± 0.09	1.00 ± 0.09	9.96 ± 4.12
ΔCBV/CBV (SE)[a]	0.79 ± 0.14	1.00 ± 0.08	5.55 ± 1.80

[a]From reference 36.

due to inadequate SNR and suboptimal *b*-values. Additionally, our DW SE sequence can have confounding effects on the functional ADC change. As shown by previous reports (30–34), coupling (or the cross-term) between the diffusion-weighting gradients and the background inhomogeneity gradients reduces the measured ADC value for a pulsed-gradient SE (PGSE) type sequence. The magnitude of this effect is dependent on the strength of the background gradients and on experimental parameters, such as TE and diffusion time. In fMRI studies using a PGSE sequence, the decrease of intravascular susceptibility during activation will cause an increase in the measured EV ADC (8). This effect is present in both the small and the large *b*-value regimes, and is expected to be more larger at high fields. This cross-term contribution to fMRI ADC measurement may cancel out any ADC-decreasing effect. We can roughly estimate how large this effect might be in our experiments assuming the ADC decrease is linearly dependent on the increase in field inhomogeneity (ΔR_2^*) (32). For typical functional ΔR_2^* values of cat visual stimulation (26), the ADC decrease due to the susceptibility effect change would not exceed 0.3% at the parenchyma and 0.5% at the cortical surface for our experimental parameters. Therefore, the contribution of the susceptibility effect to the ADC measurement (especially at the parenchyma) is expected to be small in our results. Nevertheless, in order to detect a weak ADC decrease in the large *b* regime, one must first minimize background susceptibility effects. For this purpose one can use a bipolar-paired PGSE sequence that utilizes a pair of bipolar gradients that are antisymmetrical about the 180° refocusing pulse (31,32). Further studies are needed to determine whether any tissue ADC change is detectable at high field using the bipolar-paired PGSE sequence or other techniques that can minimize the contribution from the susceptibility effect.

Arterial and Venous Blood

In our 9.4 T studies the functional ADC change from the tissue pool was minimal, and therefore the changes mostly arose from the arterial and venous blood pools. In the small *b*-value regime, the relative contributions of the arterial and venous compartments to the ADC response were drastically different due to their different T_2 values at 9.4 T. Since T_2 of arterial blood is similar to that of tissue (40 ms), the contribution from the change of arterial blood volume and flow to the ADC response is nearly TE-independent. In contrast, T_2 of venous blood is much shorter (~6 ms) than tissue T_2, and the contribution from the venous blood signal change is therefore strongly dependent on TE (it is negligible for long TE (>40 ms), and increases to a peak at a TE value of 10–15 ms (15)). At TE = 28 or 60 ms, there is small or negligible intravascular BOLD signal change from venous blood, and the ADC change mostly comes from a change in arterial blood flow and volume. Since an elevation of arterial blood volume would increase ADC (Fig. 1a), and an increase in velocity (or D_a*) would decrease it (Fig. 1e), the observed small positive ADC change suggests that an arterial CBV increase is more dominant than a velocity increase. According to our simulation, an increase in D_v^* would decrease the ADC for voxels containing mainly large vessels with large D_v^*, but would increase the ADC for those containing microvessels, including postcapillary venules and capillaries. It should be noted that this transition point of the D^* value is dependent on the two *b*-values used for the ADC measurement. Using computer simulations, Song et al. (5) observed similar effects of a blood velocity increase on ADC changes.

At a TE of 16 ms, both arterial and venous blood signals contribute to the ADC change. The venous blood contribution is more prominent at the area with large surface vessels, due to a higher baseline V_v. Since the arterial volume contribution to the functional ADC change is almost TE-independent, the difference between ADC values measured at 60 ms (with minimal venous blood contribution) and 16 ms is likely due to an increase in venous oxygenation level. Our simulations indicate that changes in venous CBV (Fig. 1b) and blood velocity (represented by D_v^*, Fig. 1f) also contribute to TE-dependent ADC changes, but with a smaller effect than venous oxygenation level changes for the three TEs used in our experiments.

At low magnetic fields, it is difficult to separate arterial and venous blood contributions to functional ADC changes when only one TE is used. Furthermore, the T_2 of arterial blood is much longer than the T_2 of tissue. Venous blood T_2 is also quite long (e.g., 90–180 ms at 1.5 T depending on *Y*) and comparable to or significantly longer than T_2 of tissue (~ 90 ms in gray matter at 1.5 T) (35). Thus, when the TE is equal to the tissue T_2 value, the contribution of arterial and venous blood is higher at low fields than at 9.4 T, and consequently the ADC change induced by both arterial and venous blood would be higher. This can partially explain the large discrepancy between the small ADC changes we observed (1–2%) and the larger values reported for human studies at 3–4 T

(8–15%), as well as the obvious differences between awake humans and anesthetized cats.

Spatial Localization of the Functional ADC Change

Since the observed functional ADC change (in the small *b*-value regime) originates mostly from the hemodynamic response rather than from a change in tissue water diffusion, the spatial localization of ΔADC/ADC should be similar to that of other hemodynamic imaging methods. To examine the relationship between ΔADC/ADC maps and conventional BOLD maps, the exact source of signal changes should be considered: ΔADC/ADC is related to changes from both arterial and venous blood, while the BOLD signal is more closely related to changes in the venous compartment. When the contribution of venous blood is suppressed (using a long-TE value at 9.4 T), ΔADC/ADC is related only to a change in arterial blood volume (and flow), which is relatively specific to the middle cortical layer (36). Indeed, the ADC response shows fairly good spatial localization to the middle cortical layer when the venous intravascular BOLD signals are suppressed (TE = 28 and 60 ms; Fig. 6b). Even when the intravascular contribution from a venous oxygenation change is significant (such as short-TE SE and typical GE studies), ΔADC/ADC should have better localization compared to BOLD signals because the CBV contribution to ΔADC/ADC is relatively specific to active neuronal sites (37). Compared to SE BOLD at 16 ms, where the highest signal change appears at the cortical surface (Fig. 6c), the improvement in ADC spatial specificity is pronounced. To improve the spatial specificity of ADC maps, it is preferable to suppress or separate the venous blood contribution. This can be achieved by using a long-TE value at high fields (≥40 ms for 9.4 T), multiple TE values, and/or the temporal characteristics of the activated pixels (14).

CONCLUSIONS

Stimulation-induced ADC changes were observed within brain parenchyma at 9.4 T using weak diffusion weighting (b = 2 and 200 s/mm^2), but the ADC changes were not observed in tissue when intravascular signals were suppressed by strong diffusion weighting (b = 200 and 800 s/mm^2). Using large *b*-values, very small ADC decreases were observed at the cortical surface; however, the source is still uncertain. With weak diffusion weighting, the observed ADC increase originated from the hemodynamic response and was highly dependent on TE. At long TE values (28 and 60 ms), the observed small ADC changes were caused mainly by a functional increase of arterial blood volume, and showed better spatial localization as compared to SE-BOLD signal changes. The TE-dependent venous BOLD signal change may contribute to the ADC change, and this contribution can be significant at lower fields. If ADC contrast is used to improve fMRI mapping, these venous BOLD contributions should be carefully separated.

ACKNOWLEDGMENTS

We thank Ping Wang and Michelle Tasker for animal preparation, Kristy Hendrich for 9.4 T support and detailed comments on the manuscript, and Dr. Allen W. Song at Duke University for valuable discussions.

REFERENCES

1. Ogawa S, Tank DW, Menon R, Ellermann JM, Kim S-G, Merkle H, Ugurbil K. Intrinsic signal changes accompanying sensory stimulation: functional brain mapping with magnetic resonance imaging. Proc Natl Acad Sci USA 1992;89:5951–5955.
2. Kwong KK, Belliveau JW, Chesler DA, Goldberg IE, Weisskoff RM, Poncelet BP, Kennedy DN, Hoppel BE, Cohen MS, Turner R, Cheng H-M, Brady TJ, Rosen BR. Dynamic magnetic resonance imaging of human brain activity during primary sensory stimulation. Proc Natl Acad Sci USA 1992;89:5675–5679.
3. Bandettini PA, Wong EC, Hinks RS, Rikofsky RS, Hyde JS. Time course EPI of human brain function during task activation. Magn Reson Med 1992;25:390–397.
4. Gangstead SL, Song AW. On the timing characteristics of the apparent diffusion coefficient contrast in fMRI. Magn Reson Med 2002;48:385–388.
5. Song AW, Woldorff MG, Gangstead SL, Mangun GR, McGarthy G. Enhanced spatial localization of neuronal activation using simultaneous apparent-diffusion-coefficient and blood-oxygenation functional magnetic resonance imaging. Neuroimage 2002;17:742–750.
6. Song AW, Harshbarger T, Li TL, Kim K-H, Ugurbil K, Mori S, Kim D-S. Functional activation using apparent diffusion coefficient-dependent contrast allows better spatial localization to the neuronal activity: evidence using diffusion tensor imaging and fiber tracking. Neuroimage 2003;20:955–961.
7. Zhong J, Petroff OAC, Pleban LA, Gore JC, Prichard JW. Reversible, reproducible reduction of brain water apparent diffusion coefficient by cortical electroshocks. Magn Reson Med 1997;37:1–6.
8. Zhong J, Kennan RP, Fulbright RK, Gore JC. Quantification of intravascular and extravascular contributions to BOLD effects induced by alteration in oxygenation or intravascular contrast agents. Magn Reson Med 1998;40:526–536.
9. Darquie A, Poline J-B, Poupon C, Saint-Jalmes H, Le Bihan D. Transient decrease in water diffusion observed in human occipital cortex during visual stimulation. Proc Natl Acad Sci USA 2001;98:9391–9395.
10. LeBihan D, Breton E, Lallemand D, Grenier P, Cabanis E, Laval-Jeantet M. MR imaging of intravoxel incoherent motions: application to diffusion and perfusion in neurologic disorders. Radiology 1986;161:401–407.
11. Le Bihan D, Urayama S, Aso T, Hanakawa T, Fukuyama H. Direct and fast detection of neuronal activation in the human brain with diffusion MRI. Proc Natl Acad Sci USA 2006;103:8263–8268.
12. Song AW, Li T. Improved spatial localization based on flow-moment-nulled and intra-voxel incoherent motion-weighted fMRI. NMR Biomed 2003;16:137–143.
13. Harshbarger T, Song AW. B factor dependence of the temporal characteristics of brain activation using dynamic apparent diffusion coefficient contrast. Magn Reson Imaging 2004;52:1432–1437.
14. Song AW, Gangstead SL. The spatial and temporal characteristics of the apparent-diffusion-coefficient-dependent fMRI signal change during visual stimulation. J Neuro Eng 2004;1:32–38.
15. Jin T, Wang P, Tasker M, Zhao F, Kim S-G. Source of nonlinearity in echo-time-dependent BOLD fMRI. Magn Reson Med 2006;55:1281–1290.
16. LeBihan D, Breton E, Lallemand D, Aubin ML, Vitnaud J, Laval-Jeantet M. Separation of diffusion and perfusion in intravoxel incoherent motion MR imaging. Radiology 1988;168:497–505.
17. Luz Z, Meiboom S. Nuclear magnetic resonance study of the protolysis of trimethyammonium ion in aqueous solution—order of the reaction with respect to solvent. J Chem Phys 1963;39:366–370.
18. Haacke EM, Lai S, Reichenbach JR, Kuppusamy K, Hoogenraad F, Takeichi H, Lin W. In vivo measurement of blood oxygen saturation using magnetic resonance imaging: a direct validation of the blood oxygen level-dependent concept in functional brain imaging. Hum Brain Mapp 1997;5:341–346.
19. Meyer M, Yu O, Eclancher B, Grucker D, Chambron J. NMR relaxation rates and blood oxygenation level. Magn Reson Med 1995;34:234–241.
20. Bryant R, Marill K, Blackmore C, Francis C. Magnetic relaxation of blood and blood clots. Magn Reson Med 1990;13:133–144.
21. Wright GA, Hu BS, Macovski A. Estimating oxygen saturation of blood in vivo with MR imaging at 1.5 T. J Magn Reson Imaging 1991;1:275–283.

22. Harel N, Lee S-P, Nagaoka T, Kim D-S, Kim S-G. Origin of negative blood oxygenation level-dependent fMRI signals. J Cereb Blood Flow Metab 2002;22:908–917.
23. Schupp DG, Merkle H, Ellermann JM, Ke Y, Garwood M. Localized detection of glioma glycolysis using edited 1H MRS. Magn Reson Med 1993;30:18–27.
24. Windischberger C, Moser E. Spatial resolution in echo planar imaging: shifting the acquisition window in k-space. Magn Reson Imaging 2000; 18:825–834.
25. Strupp JP. Stimulate: a GUI based fMRI analysis software package. Neuroimage 1996;3:S607.
26. Zhao F, Wang P, Kim S-G. Cortical depth-dependent gradient-echo and spin-echo BOLD fMRI at 9.4T. Magn Reson Med 2004;51:518–524.
27. Bonhoeffer T, Grinvald A. The layout of iso-orientation domains in area 18 of cat visual cortex: optical imaging reveals a pin-wheel-like organization. J Neurosci 1993;13:4157–4180.
28. Tsao J. Interpolation artifacts in multimodality image registration based on maximization of mutual information. IEEE Trans Med Imaging 2003;22:854–864.
29. Payne BR, Peters A. The concept of cat primary visual cortex. In: Payne BR, Peters A, editors. The cat primary visual cortex. New York: Academic Press; 2002. p 1–129.
30. Stejskal EO, Tanner JE. Spin diffusion measurements: spin echoes in the presence of a time-dependent field gradient. J Chem Physics 1965; 42:288–292.
31. Hong X, Dixon WT. Measuring diffusion in inhomogeneous systems in imaging mode using antisymmetric sensitizing gradients. J Magn Reson 1992;99:561–570.
32. Does MD, Zhong J, Gore JC. In vivo measurement of ADC change due to intravascular susceptibility variation. Magn Reson Med 1999;41:236–240.
33. Zhong J, Kennan RP, Gore JC. Effects of susceptibility variations on NMR measurements of diffusion. J Magn Reson 1991;95:267–280.
34. Kiselev VG. Effects of magnetic field gradients induced by microvasculature on NMR measurements of molecular self-diffusion in biology tissues. J Magn Reson 2004;170:228–235.
35. Golay X, Silvennoinen M, Zhou J, Clingman CS, Kauppinen RA, Pekar J, van Zijl PC. Measurement of tissue oxygen extraction ratios from venous blood T2: increased precision and validation of principle. Magn Reson Med 2001;46:282–291.
36. Zhao F, Wang P, Hendrich K, Ugurbil K, Kim S-G. Cortical layer-dependent BOLD and CBV responses measured by spin-echo and gradient-echo fMRI: insights into hemodynamic regulation. Neuroimage 2006:1149–1160.
37. Zhao F, Wang P, Hendrich K, Kim S-G. Spatial specificity of cerebral blood volume-weighted fMRI responses at columnar resolution. Neuroimage 2005;27:416–424.
38. Thulborn KR, Waterton JC, Mattews PM, Radda GK. Oxygenation dependence of the transverse relaxation time of water protons in whole blood at high field. Biochem Biophys Acta 1982;714:265–270.
39. Herscovitch P, Raichle ME. What is the correct value for the brain-blood partition coefficient for water? J Cereb Blood Flow Metab 1985; 5:65–69.
40. Lee S-P, Silva AC, Ugurbil K, Kim S-G. Diffusion-weighted spin-echo fMRI at 9.4 T: microvascular/tissue contribution to BOLD signal change. Magn Reson Med 1999;42:919–928.